phys. stat. sol. (b) **209**, 135 (1998)

Subject classification: 61.10.Nz; 75.30.Cr; 75.50.Pp; S8.16

Crystallographic and Magnetic Properties of $Cu_2FeGeSe_4$ and $Cu_2FeGeTe_4$ Compounds

M. QUINTERO (a), R. TOVAR (a), A. BARRETO (a), E. QUINTERO (a), A. RIVERO (a), J. GONZALEZ (a), G. SÁNCHEZ PORRAS (a), J. RUIZ (a), P. BOCARANDA (a), J. M. BROTO (b), H. RAKOTO (b), and R. BARBASTE (b)

(a) Centro de Estudios de Semiconductores, Departamento de Física, Facultad de Ciencias, Universidad de Los Andes, Mérida 5101, Venezuela

(b) LPMC-SNCMP INSA Complexe Scientifique de Rangueil, F-31077 Toulouse-Cedex, France

(Received April 17, 1998)

X-ray powder diffraction measurements, at room temperature, and magnetic susceptibility χ measurements, in the temperature range from 2 to 300 K, were made on polycrystalline samples of $Cu_2FeGeSe_4$ and $Cu_2FeGeTe_4$ magnetic semiconductor compounds. Magnetization measurements at 2, 4.2 and 77 K in magnetic fields up to 35 T were carried out on $Cu_2FeGeSe_4$ compounds. From the analysis of the X-ray diffraction lines, it was found that $Cu_2FeGeSe_4$ and $Cu_2FeGeTe_4$ have, respectively, stannite and monoclinic structures. The resulting $1/\chi$ versus T curves showed that $Cu_2FeGeSe_4$ is antiferromagnetic with a Néel temperature $T_N = 20$ K while $Cu_2FeGeTe_4$ is ferrimagnetic with $T_N = 160.1$ K. The magnetization and susceptibility results obtained on $Cu_2FeGeSe_4$ showed the presence of bound magnetic polarons (BMPs) in agreement with earlier studies made on this type of materials [1, 2].

1. Introduction

Magnetic semiconducting materials are of interest because of the manner in which the magnetic behavior associated with the concerned magnetic ion can modify and complement the semiconductor properties [3]. The materials that have been most studied are the semimagnetic semiconductor alloys obtained from the tetrahedrally coordinated II–VI semiconductor compounds by replacing a fraction of the group II cations with manganese, giving alloys which show spin-glass behavior, very large magneto-optical effects, etc. [3]. It was recently suggested [1, 4, 5] that another set of magnetic compounds and alloys, which could show a larger magneto-optical effect than the II–VI-derived alloys, can be obtained from the tetrahedrally bonded I_2–II–IV–VI_4 compounds by replacing the II cations by Mn, Fe, Co and/or Ni ions. The crystal structure of various I_2–II–IV–VI_4 compounds has been investigated by several workers [6 to 10], and it has been indicated that three tetrahedral structure types exist: 1. the stannite tetragonal structure based on zincblende, 2. an orthorhombic superstructure derived from wurtzite (known as wurtz-stannite) and 3. an unknown structure type based on slightly deformed tetragonal, orthorhombic or monoclinic symmetry. However, in the case of compounds involving Fe ions, only those with Cu and S or Se have been investigated, and no crystallographical study has been made on Fe materials containing Te.

With regard to the magnetic properties of these I_2–II–IV–VI_4 compounds, most of the studies have been carried out on materials involving Mn atoms, and little work is made on compounds containing Fe, viz. $Cu_2FeGeSe_4$ and $Cu_2FeGeTe_4$. Guen and Glaunsinger [11] studied the magnetic properties of Cu_2MnSiS_4, Cu_2MnGeS_4, $Cu_2MnGeSe_4$, $Cu_2FeGeSe_4$, Cu_2MnSnS_4 and $Cu_2MnSnSe_4$. Their results showed that the first five compounds were antiferromagnetic, while the $Cu_2MnSnSe_4$ one was ferromagnetic. In a recent work [12], the form of the magnetic susceptibility as a function of temperature was investigated for 19 I_2–Mn–IV–VI_4 samples with I = Cu, Ag, IV = Si, Ge, Sn, Pb and VI = Se, Te. The resulting data indicated that seven of these were antiferromagnetic, while the other 12 compounds showed ferrimagnetic behavior.

In more recent studies, made of the antiferromagnetic Cu_2MnGeS_4 compound [1] and also on the $Cu_2Mn_{0.9}Zn_{0.1}SnS_4$ alloy [2], it was found that the presence of charge carriers (holes in these cases) leads to an indirect Mn–Mn ferromagnetic interaction, i.e. formation of bound magnetic polarons (BMPs) near the occupied acceptors, which affects the magnetic properties of these materials such as low-field susceptibility and magnetization curves at low temperature.

In the present program of work, the properties of some I_2–II–IV–VI_4 compounds with I = Cu, Ag, II = Mn, Fe, IV = Si, Ge, Sn, Pb and VI = Se, Te are being studied. The aim of this paper is to show some results of the initial work on the crystallographic and magnetic properties of these materials. Here, results of X-ray powder diffraction, at room temperature, magnetic susceptibility as a function of temperature and magnetization at various temperatures are presented for $Cu_2FeGeSe_4$ and $Cu_2FeGeTe_4$ compounds.

2. Sample Preparation and Experimental Techniques

The samples used were prepared by the melt and annealing technique. In each case, components of 1 g sample were made from appropriate amounts of the elements and were sealed under vacuum in small quartz ampoules, which had previously been carbonized to prevent the interaction of the components with quartz. The components were melted together at 1150 °C for about 1 h, annealed to equilibrium at 500 °C, then cooled to room temperature by leaving the ampoule in the switched-off furnace. In each case, a Guinier X-ray powder photograph using CuKα ($\lambda = 1.5406$ Å) radiation was taken of the prepared sample to check the equilibrium conditions as well as the presence of secondary phases in the compound. It was found that an annealing period from twenty to thirty days produces specimens with good equilibrium conditions. Using a Perkin Elmer DTA-7 equipment, differential thermal analysis runs were taken on each sample prepared. The obtained cooling DTA melting peaks of the samples are shown in Figs. 1a and b. The melting points were found to be 733 and 692 °C for $Cu_2FeGeSe_4$ and $Cu_2FeGeTe_4$, respectively.

Resistivity measurements were made on a small slice of about 0.5 mm thickness cut from the $Cu_2FeGeSe_4$ ingot used in this work. Ohmic electrical contacts to the sample were made by electroplating four symmetrical copper spots, which were used as a base for soldering copper leads with indium. These measurements were made with the van der Pauw method using dc current.

For each compound, magnetic susceptibility measurements as a function of the temperature T in the range 2 to 300 K were made using a Quantum Design SQUID mag-

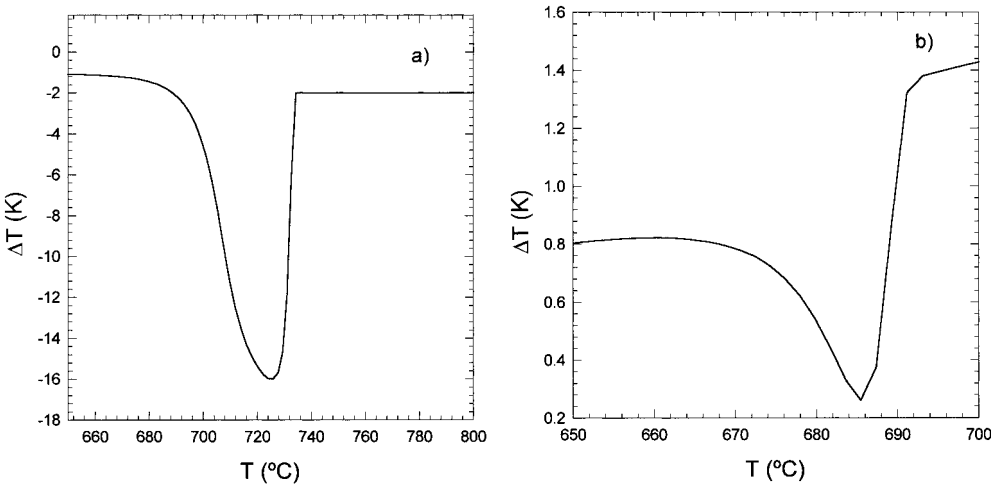

Fig. 1. Cooling DTA thermogram for a) $Cu_2FeGeSe_4$ and b) $Cu_2FeGeTe_4$

netometer with an external magnetic field of 100×10^{-4} T. The resulting $1/\chi$ versus T curves were analyzed to determine both the magnetic interactions between the Fe ions and the values of the various magnetic parameters when it was possible, as discussed below.

In the case of the $Cu_2FeGeSe_4$ compound, magnetization M measurements were performed using the high magnetic field facilities in Toulouse. The field is produced by the discharge of a capacitor bank in a resistive copper coil. The maximum field (35 T) is reached within 100 ms and the decreasing time is 300 ms. In order to measure the magnetization, two pick up coils are mounted to give zero induced voltage in absence of the sample. The signal in the presence of sample is proportional to the derivative of its magnetization.

3. Results and Discussion

3.1 X-ray results and analysis

The Guinier X-ray powder photographs showed sharp diffraction lines indicating that the samples were in good equilibrium conditions. The diffraction patterns, obtained for each compound, were indexed with the computer program DICVOL91 [13] using an absolute error of 0.03° (2θ) in the calculations. In the case of the $Cu_2FeGeSe_4$ compound, the X-ray pattern showed the stannite tetragonal structure ($I\bar{4}2\,m$) and no traces of secondary phases were observed. The obtained lattice parameter values were $a = (5.5906 \pm 0.00153)$ Å and $c = (11.0300 \pm 0.0168)$ Å, these results are in good agreement with those reported by Schafer and Nitsche [9]. It is to be noted that the ratio $c/a = 1.97$ gives a tetragonal distortion along the z-axis ($\delta = 2 - c/a$) of 0.03, a value similar to the case of the I–III–VI_2 chalcopyrite compounds [14]. For the $Cu_2FeGeTe_4$ compound, no crystallographic data have been reported for this material so far. The corresponding diffraction pattern was indexed as indicated above and it was found that the best solution produced by the program showed a monoclinic structure with crystal parameter values of $a = (10.3129 \pm 0.0038)$ Å, $b = (4.0352 \pm 0.0012)$ Å,

Table 1
X-ray powder diffraction data for $Cu_2FeGeTe_4$
$a = 10.3129$ Å, $b = 4.0352$ Å, $c = 7.4345$ Å, $\beta = 89.261°$

$2\theta_{obs}$	d_{obs} (Å)	$(I/I_0)_{obs}$	h	k	l	$2\theta_{cal}$	d_{cal} (Å)	$\Delta 2\theta$
14.590°	6.0664	10	1	0	1	14.587°	6.0675	0.003°
25.890°	3.4386	90	3	0	0	25.900°	3.4373	−0.010°
26.510°	3.3596	80	1	1	1	26.506°	3.3600	0.004°
29.780°	2.9977	100	2	0	−2	29.788°	2.9969	−0.008°
30.640°	2.9154	5	2	1	−1	30.660°	2.9136	−0.020°
33.960°	2.6377	30	1	1	−2	33.977°	2.6364	−0.017°
35.310°	2.5399	5	3	0	2	35.308°	2.5400	0.002°
42.010°	2.1490	50	3	1	2	41.997°	2.1496	0.013°
42.940°	2.1046	50	4	0	−2	42.916°	2.1057	0.024°
43.210°	2.0920	50	4	1	1	43.224°	2.0914	−0.014°
44.900°	2.0171	40	0	2	0	44.889°	2.0176	0.011°
71.120°	1.3245	10	2	2	4	71.129°	1.3244	−0.009°

$M_{12} = 16.3$ $F_{12} = 6.2$ (0.0112,174)

$c = (7.4345 \pm 0.0041)$ Å and $\beta = (89.261 \pm 0.025)°$. In Table 1 the resulting X-ray powder diffraction data together with the visual intensity I/I_0 values of the reflection lines and the de Wolf [15] and Smith-Snyder [16] figures of merit are listed. It is to be mentioned that the X-ray powder diffraction photograph of this compound also contained additional weak diffraction lines which could be explained as due to the presence of $FeTe_2$ (PDF 14-419) as secondary phase. In fact, the X-ray powder diffraction photographs taken of each I_2–Fe–IV–Te_4 sample prepared in this program showed traces of this $FeTe_2$ secondary phase, moreover, these traces were also observed in compounds such as $CuFeTe_2$, $AgFeTe_2$, $MnFe_2Te_4$ and $FeMn_2Te_4$, this will be discussed in further work.

3.2 Electrical transport

The conductivity of $Cu_2FeGeSe_4$, as checked by a thermal probe, was found to be p-type. Typical electrical parameter values at RT are 0.57 Ω cm, 1.1×10^{19} cm^{-3} and 0.98 cm^2/Vs for the resistivity, hole concentration and mobility, respectively. The resistivity ϱ was measured in the temperature range from 100 to 300 K and the resulting ϱ versus $1000/T$ curve is shown in Fig. 2. It is seen that, within the limits of experimental error, this variation appears to be nearly linear and that ϱ increases as T is decreased. The hole binding energy E_h was estimated from the slope of the $\ln(\varrho)$ versus $1000/T$ curve, and the resulting value was found to be $E_h \approx 42$ meV, with an uncertainty of about 10%. These shallow acceptor levels favor the presence of BMPs in this sample.

3.3 Magnetic susceptibility results and analysis

The obtained $1/\chi$ versus T curve for $Cu_2FeGeSe_4$ is shown in Fig. 3. It can be seen from this figure that the $1/\chi$ versus T graph is linear at higher temperatures, but shows deviation from the Curie-Weiss form for temperatures below 100 K. As it was indicated above, this deviation is due to the presence of free carriers which could lead to the formation of BMPs [1 to 4], this will be discussed below. For antiferromagnetic

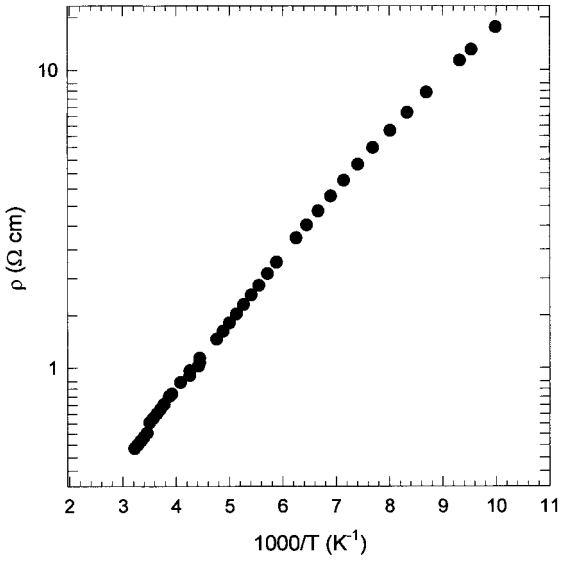

Fig. 2. Variation of the resistivity ϱ with T for $Cu_2FeGeSe_4$

behavior, the variation of $1/\chi$ with T well above the Néel temperature is given by the relation

$$\frac{1}{\chi} = \frac{(T - \theta_a)}{C}\,, \tag{1}$$

where θ_a is the Curie-Weiss temperature and C the Curie constant, while the minimum in $1/\chi$ at lower temperatures gives the Néel temperature T_N. The theoretical value of C is given by [17]

$$C = \frac{N_A g^2 \mu_B^2 J(J+1)}{3k_B W}\,, \tag{2}$$

where N_A is the Avogadro number, μ_B the Bohr magneton and W the molecular weight. Thus, the experimental data for $T \geq 150$ K in Fig. 3 were fitted to the above equation and the obtained results were $C = 9.77 \times 10^{-3}$ emu K/g and $\theta_a = -155.05$ K. The experimental value of C is close to the theoretical value $C = 9.82 \times 10^{-3}$ emu K/g, obtained from eq. (2) using $J = 4$ and a g-factor of 1.5 for the Fe^{2+} ion. No values of C and θ_a have been quoted for this compound in the literature.

The zero-field cooling and field cooling susceptibility χ results for $T < 50$ K for the $Cu_2FeGeSe_4$ compound are illustrated in Fig. 4. Fig. 5 shows the obtained M versus B curves at 2, 4.2 and 77 K. It is seen from Fig. 4, that the susceptibility measurements carried out under zero-field cooling and field cooling gave identical results, so that spin-glass behavior is ruled out here. Also, it is observed from this fig-

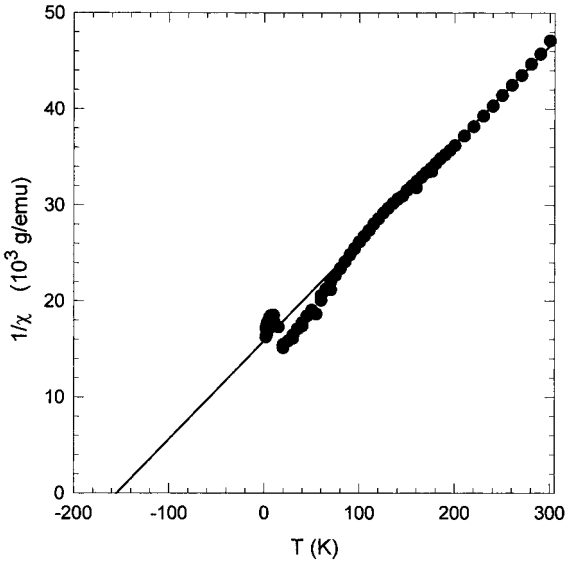

Fig. 3. Variation of $1/\chi$ with T for $Cu_2FeGeSe_4$. Full circles: experimental data; full line: line fitted to eq. (1)

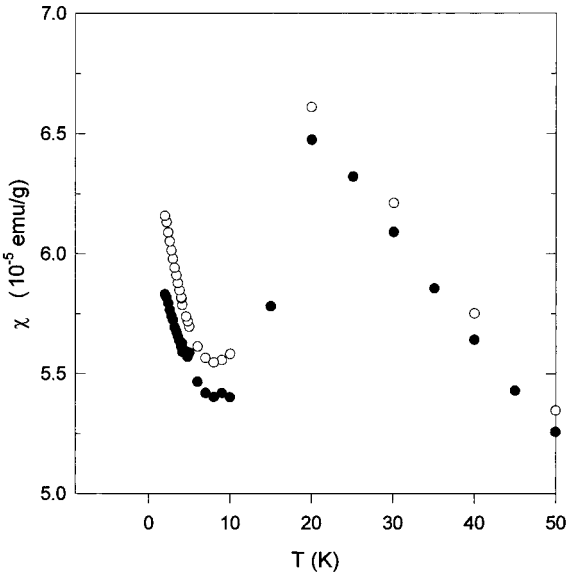

Fig. 4. Variation of ZFC (●) and FC (○) low field susceptibility χ with T for $Cu_2FeGeSe_4$

ure that below 50 K the susceptibility increases with decreasing T until the peak in χ at 20 K, which is identified as the Néel temperature T_N, occurs. Then, below 7 K the susceptibility increases again with decreasing T. As indicated above, this behavior can be attributed to the sp–d coupling between the spins of the charge carriers (holes or electrons) and those of the Fe ions, leading to an indirect Fe–Fe ferromagnetic interaction affecting the magnetic properties. As the temperature is lowered the free carriers may become localized near impurities. Then, as the present sample is p-type, the p–d interaction may give origin to the formation of ferromagnetic clusters near such impurities, i.e. bound magnetic polarons (BMPs) [1 to 4], which enhances the low-field susceptibility at low T.

Another point that supports this interpretation is the rapid rise of M observed in Fig. 5 at low field, for the curves obtained at 2 and 4.2 K, which is attributed to BMPs associated with holes bound to acceptors. The much slower magnetization rise above 2 T is due to the d spins outside the BMPs. Hence, the contribution of the BMPs and that of the matrix to the magnetization can be separated. However, as the temperature increases the BMPs rise more slowly and it becomes difficult to observe the BMP contribution, this is consistent with the M versus field curve at 77 K shown in Fig. 5. A similar behavior was observed by Shapira

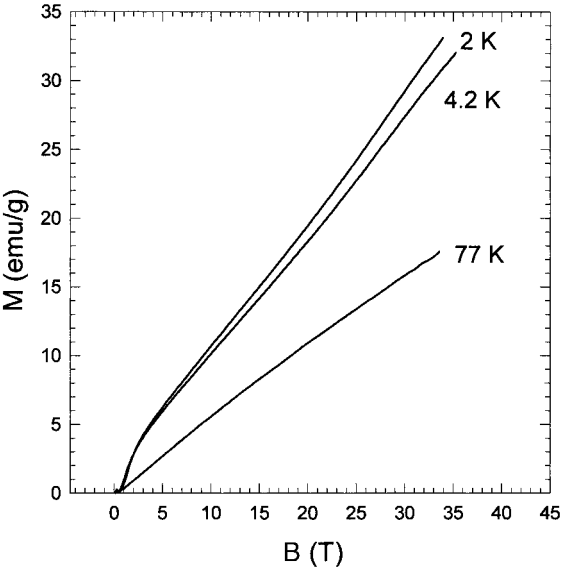

Fig. 5. Isothermal magnetization M vs. B curves for $Cu_2FeGeSe_4$

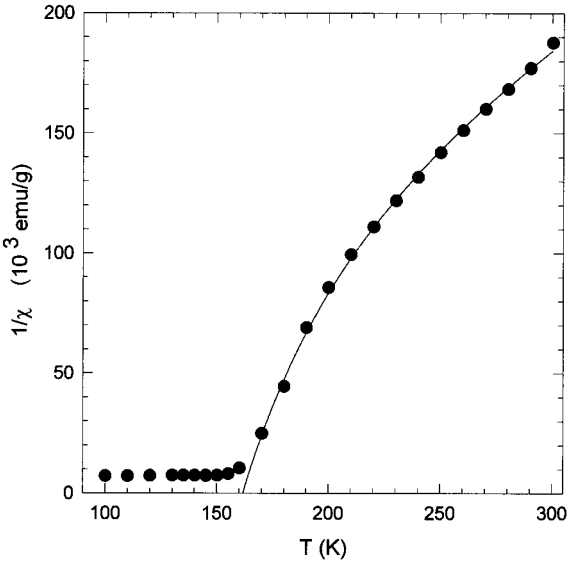

Fig. 6. Variation of $1/\chi$ with T for $Cu_2FeGeTe_4$. Full circles: experimental data, full curve: curve fitted to eq. (4)

et al. [1] on a p-type Cu_2MnGeS_4 crystal sample grown by chemical vapor transport (CVT) and by McCabe et al. [2] on a p-type $Cu_2Mn_{0.9}Zn_{0.1}SnS_4$ alloy. Also, it is to be mentioned that previous experiments on EuTe samples with electron concentration of 1.1×10^{19} cm^{-3} at 300 K showed that the low-field susceptibility for temperatures T near to T_N was much larger than for insulating samples and below T_N the susceptibility did not vary monotonically with T [18]. These results are consistent with the present data. A quantitative analysis that separates the matrix and BMP contributions to M for $Cu_2Cd_{1-z}Fe_zGeSe_4$ alloys will be presented in a further work.

Turning to the $Cu_2FeGeTe_4$ sample, the $1/\chi$ versus T curve obtained for this compound is illustrated in Fig. 6. It is seen that this curve has a form which is typical of a ferrimagnetic material and no effects from the secondary $FeTe_2$ antiferromagnetic ($T_N = 83$ K) phase [19] to this curve are observed in the temperature range investigated here. However, the X-ray data indicate that in the sample analyzed the amount of the second phase present was a few percent, so that the effect due to inaccuracy of the mass m of the material to the susceptibility measurements is very small. Hence, the contribution due to the presence of this phase is negligible and will not be considered in the present analysis. At this stage, it is not possible to rule out other effects such as canted antiferromagnetism and weak ferromagnetism behaviors proposed by Dzialoshinsky [20] and Moriya [21, 22]. However, the present $1/\chi$ versus T curve seems to have a form closer to that of Néel ferrimagnetism than to these latter cases.

From the Néel theory of ferrimagnetism, the variation of the magnetic susceptibility χ with temperature T in the range $T > T_N$ is given by the relation [17]

$$\frac{1}{\chi} = \frac{T - \theta_a}{C} - \frac{\zeta}{T - \theta}, \tag{3}$$

where θ_a is the asymptotic Curie-Weiss temperature, C is the Curie constant, and ζ and θ are parameters that depend upon the magnetic ion concentration, exchange interaction, etc. Considering that $1/\chi$ is effectively zero at $T = T_N$, the Néel temperature, eq. (3) can be rewritten as

$$\frac{C}{\chi} = T - \theta_a - \frac{(T - \theta_a)(T_N - \theta)}{T - \theta}. \tag{4}$$

Thus, using the value of $C = 7.344 \times 10^{-3}$ emu K/g determined from eq. (2) with θ_a, θ and T_N as unknown parameters, a fit of the experimental curve in Fig. 5 to eq. (4) was made for $T \geq 170$ K. It was found that a good fit could be obtained giving parameter values of $\theta_a = (-1986.30 \pm 34.60)$ K, $\theta = (73.45 \pm 3.63)$ K and $T_N = (162.30 \pm 0.40)$ K, the resulting fitted curve is shown in Fig. 6. When C together with θ_a, θ and T_N are treated as unknown parameters, a similar good fit to the $1/\chi$ versus T curve was found, but the values of C and θ_a were found to be smaller than those given above, while the values of T_N obtained from both fits are very similar and close to the value that can be estimated from inspection of the $1/\chi$ versus T curve. In eq. (3) the term $\zeta/(T - \theta)$ should become negligible for T values appreciably larger than T_N. However, because of the upper limit of $T = 300$ K available in the present experimental measurements, it was found that the $\zeta(T - \theta)$ term still contributed to some extent to $1/\chi$, even at the highest temperature of observation, so that although T_N can be determined, a reliable value of θ_a cannot be obtained from fitting eq. (4) to the experimental data in Fig. 6.

4. Conclusions

The X-ray results showed that the $Cu_2FeGeSe_4$ compound has the expected tetragonal stannite structure, with crystal parameter values in good agreement with those given earlier, while the $Cu_2FeGeTe_4$ compound was found to have a monoclinic structure. Also, the X-ray pattern obtained for this compound showed additional lines due to the $FeTe_2$ secondary phase.

The magnetic data showed that the $Cu_2FeGeSe_4$ compound is antiferromagnetic, and that there is a contribution arising from BMPs, which affect the susceptibility at low temperature. A detailed analysis of BMPs on this type of material will be given elsewhere. It is to be noted that the saturation field was not reached in the present measurements. The theoretical saturation value, assuming $J = 4$ and $g = 1.5$ for Fe^{2+}, is 58 emu/g, hence magnetization measurements in magnetic fields up to 61 T are being performed on this compound. In the case of the $Cu_2FeGeTe_4$ compound, the magnetic behavior can be fitted using the Néel relation for ferrimagnetism. Nevertheless, because of the upper limit of $T = 300$ K available in the present measurements a reliable value of θ_a could not be determined. However, it is to be pointed out that other mechanisms can give similar χ versus T curves, such as the canted antiferromagnetism (or weak ferromagnetism) [20 to 22]. These effects can occur in low-symmetry crystalline systems, which could be the case of this compound. The main difference between ferrimagnetism and canted antiferromagnetism is that in the former, magnetic ions need to be present on non-equivalent crystallographic sites, while for the latter case crystallographically equivalent sites are postulated. Hence, in order to take this analysis further, it is required to have more detailed information on the crystal structure. For this, it is planned to determine the crystal structure using single-crystal X-ray and neutron diffraction methods, as well as to carry out Mössbauer measurements.

Acknowledgements This work was supported by CONICIT-BID under grant NM-09 and CDCHT of the Universidad de Los Andes. One of the authors (M.Q.) is grateful to the CEFI-PCP Materials (France) for financial support and also for the hospitality during his stay at LPMC-SNCMP INSA (Toulouse, France).

References

[1] Y. Shapira, E. J. McNiff, Jr., N. F. Oliveira, Jr., E. D. Honig, K. Dwight, and A. Wold, Phys. Rev. B **37**, 411 (1988).
[2] G. H. McCabe, T. Fries, M. T. Liu, Y. Shapira, L. R. Ram-Mohan, R. Kershaw, A. Wold, C. Fau, M. Averous, and N. F. McNiff, Jr., Phys. Rev. B **56**, 6673 (1997).
[3] J. K. Furdyna and J. Kossut, Diluted Magnetic Semiconductors, Semiconductors and Semimetals, Eds. R. K. Willardson and A. C. Beer, Vol. 25, Chap. 1, Academic Press, New York 1988.
[4] P. A. Wolf, D. Heimann, E. D. Isaac, P. Becla, S. Foner, I. R. Ram-Mohan, D. H. Ridgley, K. Dwight, and D. Wold, High Magnetic Fields in Semiconductor Physics, Ed. G. Landwehr, Springer-Verlag, Berlin 1988.
[5] P. A. Wolff and L. R. Ram-Mohan, Mater. Res. Soc. Symp. Proc. **89**, 1 (1987).
[6] R. Nitsche, D. F. Sargent, and P. Wild, J. Cryst. Growth **1**, 52 (1967).
[7] E. Parthé, K. Yvon, and R. H. Deich, Acta Cryst. **B25**, 1164 (1969).
[8] J. Allemand and M. Wintenberg, Bull. Soc. Franç. Minéral. Crist. **93**, 14 (1970).
[9] W. Schafer and R. Nitsche, Mater. Res. Bull. **9**, 645 (1974).
[10] J. C. Woolley, G. Lamarche, A.-M. Lamarche, and M. Quintero, Crystallography and Magnetic Behaviour of Some I_2–Mn–IV–VI_4 Compounds, Proc. 8th Internat. Conf. Ternary and Multinary Compounds (ICTMC), Kishinev (URSS), 1990, Eds. S. I. Radausan and C. Shewab, Izd. Shtiintsa, 1992.
[11] L. Guen and W. S. Glaunsinger, J. Solid State Chem. **35**, 10 (1980).
[12] X. L. Chen, A.-M. Lamarche, G. Lamarche, and J. C. Woolley, J. Magn. Magn. Mater. **118**, 119 (1993).
[13] A. Boultif and D. Louer, J. Appl. Cryst. **24**, 987 (1991).
[14] J. L. Shay and J. H. Wernick, Ternary Chalcopyrite Semiconductors: Growth, Electronic Properties and Applications, Pergamon Press, Oxford 1974.
[15] P. M. De Wolff, J. Appl. Cryst. **5**, 108 (1968).
[16] G. S. Smith and R. L. Snyder, J. Appl. Cryst. **12**, 60 (1979).
[17] J. S. Smart, Effective Field Theories of Magnetism, Saunders, Philadelphia 1966 (pp. 60, 113).
[18] N. F. Oliveira, Jr., S. Foner, Y. Shapira, and T. B. Reed, Phys. Rev. B **5**, 2634 (1972).
[19] J. H. Zhand, B. Wu, C. J. Oconnor, and W. B. Simmons, J. Appl. Phys. **73**, 571 (1993).
[20] I. E. Dzialoshinsky, J. Phys. Chem. Solids **4**, 241 (1958).
[21] T. Moriya, Phys. Rev. **117**, 635 (1960).
[22] T. Moriya, Phys. Rev. **120**, 91 (1960).